

Characterization of a *Bacillus subtilis* transporter for petrobactin, an anthrax stealth siderophore

Anna M. Zawadzka^a, Youngchang Kim^{b,1}, Natalia Maltseva^b, Rita Nichiporuk^a, Yao Fan^b, Andrzej Joachimiak^b, and Kenneth N. Raymond^a

^aDepartment of Chemistry, University of California, Berkeley, CA 94720-1460; and ^bBiosciences Division, Midwest Center for Structural Genomics, Argonne National Laboratory, Argonne, IL 60439

Edited by Joan Selverstone Valentine, University of California, Los Angeles, CA, and approved October 13, 2009 (received for review May 20, 2009)

Iron deprivation activates the expression of components of the siderophore-mediated iron acquisition systems in *Bacillus subtilis*, including not only the synthesis and uptake of its siderophore bacillibactin but also expression of multiple ABC transporters for iron scavenging using xenosiderophores. The *yclNOPQ* operon is shown to encode the complete transporter for petrobactin (PB), a photoreactive 3,4-catechololate siderophore produced by many members of the *B. cereus* group, including *B. anthracis*. Isogenic disruption mutants in the *yclNOPQ* transporter, including permease YclN, ATPase YclP, and a substrate-binding protein YclQ, are unable to use either PB or the photoproduct of FePB (FePB^o) for iron delivery and growth, in contrast to the wild-type *B. subtilis*. Complementation of the mutations with the copies of the respective genes restores this capability. The YclQ receptor binds selectively iron-free and ferric PB, the PB precursor, 3,4-dihydroxybenzoic acid (3,4-DHB), and FePB^o with high affinity; the ferric complexes are seen in ESI-MS, implying strong electrostatic interaction between the protein-binding pocket and siderophore. The first structure of a Gram-positive siderophore receptor is presented. The 1.75-Å crystal structure of YclQ reveals a bilobal periplasmic binding protein (PBP) fold consisting of two $\alpha/\beta/\alpha$ sandwich domains connected by a long α -helix with the binding pocket containing conserved positively charged and aromatic residues and large enough to accommodate FePB. Orthologs of the *B. subtilis* PB-transporter YclNOPQ in PB-producing *Bacilli* are likely contributors to the pathogenicity of these species and provide a potential target for antibacterial strategies.

crystal structure | substrate-binding protein | Gram-positive bacteria | iron

For aerobic bacteria, acquisition of iron, an essential micronutrient, poses a particular challenge because [Fe³⁺] is poorly bioavailable due to its insolubility as hydroxy oxides. In vivo iron pools are tightly regulated, and Fe³⁺ is bound to transport and storage proteins within cells and extracellular compartments (1). To compete, microorganisms, particularly human pathogens, evolved multiple means of obtaining iron. These systems are essential for bacterial survival and pathogenicity (2). Siderophores are low molecular weight, high-affinity iron chelators secreted in response to iron limitation to scavenge iron, and their acquisition systems are the most diverse and broadly distributed iron uptake mechanisms of microorganisms. Much more is known about these systems in Gram-negative than in Gram-positive bacteria. In Gram-positive bacteria, including *Bacillus* species, ferric siderophores are first bound by specific membrane-anchored substrate-binding proteins (SBPs), which are related to the periplasmic binding proteins (PBPs) of Gram-negative bacteria. Ferric siderophores are then transported across the cytoplasmic membrane through the permease component of the ABC-type transporters in a process energized by ATP hydrolysis in the transporter ATPase domain (3). To adapt to variable environmental conditions, microorganisms usually produce more than one siderophore and commonly carry genes encoding transporters for several other xenosiderophores in addition to the ones produced endogenously (2).

Bacillus subtilis is the prototypical Gram-positive bacterium, and recent studies of its iron metabolism have elucidated multiple

aspects of siderophore synthesis, transport, and regulation (4–8). *B. subtilis* produces bacillibactin (BB), a 2,3-dihydroxybenzoyl-Gly-Thr trilactone siderophore (Fig. 1) (9), and expresses a BB-specific ABC transporter FeuABC-YusV (6). Additionally, transporters specific for exogenous siderophores, including ferric citrate, ferri-chromes (Fch), ferrioxamines, and citrate-based hydroxamates, have been identified (7, 10). Our previous studies determined that *B. subtilis* can also use petrobactin (PB) for iron acquisition via a receptor different from the BB transporter (11).

First found as a siderophore produced by marine bacteria (12), PB is also synthesized by members of the *B. cereus* group, including the anthrax pathogen *B. anthracis* (Fig. 1) (13–15). PB is a crucial virulence component of *B. anthracis* that enables the bacteria to establish infection in mice and supports development in macrophages (16). The innate immune protein siderocalin protects a potential host from infections caused by pathogens by binding many bacteria-secreted siderophores. However, the presence of 3,4-catechololate units precludes binding of PB by siderocalin, which enables PB-producing bacteria to evade the host immune response (17, 18). The citrate backbone also makes the FePB complex photoreactive, resulting in decarboxylation and reduction of the iron center. The product of FePB photolysis (FePB^o) remains a powerful ferric chelator and can still be used by *B. subtilis* as an iron source (11). What is the uptake pathway of PB and how is it distinct from other siderophores not associated with virulence?

Because siderophore transporters constitute an attractive target for the development of strategies against infections caused by bacteria (19), we aimed to identify the PB transporter in *B. subtilis*, the most-studied representative of the genus *Bacillus*. We report here characterization of the PB uptake system YclNOPQ in *B. subtilis*. We also present the crystal structure of the SBP YclQ that has been determined at 1.75 Å. To understand the binding of a substrate molecule FePB to YclQ, the comparative analysis of conserved residues in the protein binding pocket is presented. This report, in combination with our study on *B. cereus* SBPs (20), gives a detailed view of virulence-related, PB-mediated iron transport systems in Gram-positive bacteria.

Results and Discussion

B. subtilis has been shown to have separate transport systems for uptake of its siderophore BB as well as several other exogenous ligands (7, 10). Previous studies identified additional Fur-regulated uptake systems of unknown substrate preference (21). Here we have shown that the *yclNOPQ* operon encodes a transporter for PB

Author contributions: A.M.Z., Y.K., N.M., A.J., and K.N.R. designed research; A.M.Z., Y.K., N.M., R.N., and Y.F. performed research; A.M.Z., Y.K., N.M., A.J., and K.N.R. analyzed data; and A.M.Z., Y.K., N.M., A.J., and K.N.R. wrote the paper.

The authors declare no conflict of interest.

This article is a PNAS Direct Submission.

Data deposition: Atomic coordinates and structure factors have been deposited in the Protein Data Bank, www.pdb.org (PDB ID code 3GFV).

¹To whom correspondence should be addressed. E-mail: ykim@anl.gov.

This article contains supporting information online at www.pnas.org/cgi/content/full/0904793106/DCSupplemental.

Table 1. Ligand binding by recombinant YclQ determined using fluorescence emission quenching and molecular weights of YclQ and its noncovalent complexes with the siderophores determined by ESI-MS

Ligand*	K_d (nM) [†]	Molecular Weight	
		Calculated [‡]	Measured [§]
—	—	33,467	33,465
PB	35 (2)	34,185	ND [¶]
Fe ^{III} (PB)	113 (4)	34,238	34,238
Fe ^{III} (PB) [‡]	142 (11)	34,192	34,193
3,4-DHB	137 (18)	33,621	ND
Fe ^{III} (3,4-DHB) ₂	4.2 (1)	33,827	33,826
Fe ^{III} (3,4-DHB)	—	33,675	ND
Fe ^{III} **	—	33,520	33,519

*3,4-DHB forms a mixture of ML and ML₂ complexes in the experimental conditions used here.

[†]The dissociation constants (K_d) were determined from fluorescence data and are the mean of at least three independent measurements with SD given in parenthesis.

[‡]Calculated masses of noncovalent complexes were computed using masses of neutral ligand species.

[§]Mass measured \pm 1 Da.

[¶]ND, not detected.

^{||}Observed in LTQ Orbitrap XL ESI-MS analysis.

**Observed in Q-TOF ESI-MS analysis.

model that allowed for determination of dissociation constants (K_d) (24). YclQ was found to bind iron-free PB with low K_d and had weaker affinity for FePB (Fig. S2 and Table 1). The affinity of YclQ for FePB[‡] is only slightly lower than for the intact ligand, indicating that photoinduced decarboxylation of FePB has little effect on binding of the complex by the receptor. The binding affinity of YclQ for FePB (113 nM) and FePB[‡] (142 nM) is weaker than the affinity reported for *B. subtilis* SBP FeuA toward FeBB (57 nM) (6) or *Staphylococcus aureus* FhuD receptors for hydroxamate siderophores (20 nM for Fch and 50 nM for FeDFO) (25). Compared with *E. coli* PBPs, the YclQ binding affinity is about 4 \times weaker than the affinity of FepB for ferric enterobactin (Ent) (30 nM), but stronger than reported for hydroxamate-binding FhuD (0.3, 0.4, 1.0, and 79 μ M for coprogen, aerobactin, Fch, and Fch A, respectively) (2). The K_d value defining the binding of YclQ to PB, a mixed 3,4-catecholate/ α -hydroxycarboxylate siderophore, is therefore in the range of the affinities displayed by other Fe-catecholate and Fe-hydroxamate transport systems. Surprisingly, however, YclQ binds apo-PB with K_d lower than the one observed for the ferric complex, which is contrary to what was determined for the binding of apo-BB by FeuA (6). Although the binding of the iron-free form of siderophores by receptor proteins was observed in other bacteria, the receptors typically have higher affinities for the ferric complex, and it is the binding of the ferric form that triggers receptor conformation changes leading to translocation of the siderophore complex (2). Therefore, our observation can be indicative of a different mechanism of PB-mediated iron uptake involving, for example, a siderophore shuttle (26). Alternatively, it can reflect a different change of the protein conformation or tryptophan environment imposed by the two forms of PB influencing quenching of protein fluorescence (20).

To determine whether ligand recognition by the YclQ receptor is dependent on the presence of 3,4-catechol functionalities, binding of 3,4-DHB was examined, as was uptake mediated by 3,4-DHB. A 1:3 ratio of iron:3,4-DHB was used that was previously confirmed to contain a mixture of ML and ML₂ complexes in our experimental conditions in neutral pH (20). The YclQ fluorescence was quenched by both iron-free 3,4-DHB and its ferric complex (Fig. S2). K_d of 4.2 ± 0.1 nM for Fe(3,4-DHB) indicates that the receptor may be at least 30-fold more specific for ferric 3,4-DHB than for FePB (Table 1). Although 3,4-DHB is secreted in large quantities

by *B. anthracis*, its role as a siderophore is unclear (27). Similar to the BB precursor itoic acid (2,3-dihydroxybenzoyl glycine) produced by *B. subtilis*, such bidentate ligands have much lower affinity for iron than the hexadentate siderophores. Although itoic acid was shown to promote iron delivery (4), recent studies have indicated that it is not capable of relieving iron limitation to the same extent as BB and is bound by FeuA with only 0.8% affinity of that of BB (6). However, because 3,4-DHB is produced at high concentrations by some *Bacilli*, and the YclQ SBP has a very high nanomolar-range affinity for this ligand, 3,4-DHB is likely to participate in iron scavenging, as suggested for *Magnetospirillum magneticum* (28). However its role in iron transport is likely auxiliary to the multi-dentate siderophores, which suggests an additional function for 3,4-DHB.

Finally, the affinity of YclQ toward 2,3-catecholates, including apo- and ferric BB, Ent, and 2,3-DHB was tested. In contrast to 3,4-DHB and PB, YclQ does not exhibit specific interactions with BB, FeBB, Ent, nor 2,3-DHB. The YclQ fluorescence was moderately quenched by FeEnt and to a much lesser extent by Fe(2,3-DHB)₃ (K_d of 534 ± 79 nM and 1.23 ± 0.1 μ M, respectively), suggesting some affinity for these ligands—albeit much less specific than for 3,4-DHB and PB (Fig. S2). Overall, YclQ shows apparent preference for 3,4-dihydroxybenzoyl-substituted ligands.

Structural Characterization of YclQ. The YclQ protein structure was determined at 1.75 Å (Table S1); it consists of the N- and C-terminal α/β domains with a ligand-binding cleft between the domains (29–32). The YclQ structure belongs to class III of PBPs as the two globular domains are connected by one long α -helix (α_5) (Fig. 44). The PBPs are a large family of proteins with low sequence homology but similar overall 3D structures, and SBPs are their membrane-tethered counterparts in Gram-positive bacteria. A small β -hairpin (β_1 –2) starts the N terminus of YclQ, which is followed by the N-terminal α/β domain containing a five-stranded (β_3 –7), all-parallel β -sheet surrounded by three 1- or 2-turn α -helices (α_1 –3) and one longer α -helix (α_4). The C-terminal domain has a twisted β -sheet of four mixed strands (β_8 –11) surrounded by six small α -helices (α_6 –11) and is completed with a longer helix (α_{12}). The α_4 and α_{12} helices of each of α/β domain and the long connecting α_5 helix form a solid backbone of the structure (Fig. 44). The closest structural YclQ homolog is the Ent-binding PBP CeuE (PDB ID 2chu) from *Campylobacter jejuni* complexed with ferric Fe³⁺(mecam)⁶⁻, an Ent analog; the sequence identity is 42%, $Z = 14.6$, and the rmsd on Ca positions is as low as 1.55 Å (30). The structures of *E. coli* PBP FhuD complexed with a number of hydroxamate siderophores, such as gallichrome (1efd), albomycin δ_2 (1k7s), coprogen (1esz), and DFO (1k2v), which are also structurally similar to YclQ with Z values near 7.0 and rmsd of 2.7 Å. However, the sequence identity is only about 17% (31, 32). There are a number of other PBP structures, including bacterial heme-binding protein (2rg7, 2r7a, and 2r79), IsdE complexed with heme (2q8q), periplasmic iron(III)-binding protein (2etv), and BtuF complexed with vitamin B12 (1n4a and 1n2z) with similarities ranging (by Z values) from 4 to 6 with rmsd's of 2.6 Å or higher, depending on the size and the ligand; however, their sequence identities to YclQ are all below 20%. The only other structure of an SBP from Gram-positive bacterium is FeuA from *B. subtilis* (PDB ID 2phz) that has similarity in shape ($Z = 7.6$ and rmsd = 2.5 Å) but only 28% sequence identity. More distantly related groups of proteins are class I and II PBPs, which possess similar N- and C-terminal α/β domains connected by short loops extended from the N- and the C-terminal β -strand sheets, which provide a flexible space for number of distinct substrates (33). YclQ belongs to the class III PBP, in which one α -helix connects the N- and the C-terminal domains presumably with less flexibility but higher specificity. Finally, the surface charge potential for N- and C-terminal α/β domain of YclQ are dissimilar (Fig. 4B); the C-terminal domain with a mixed-stranded β -sheet contains a distinc-

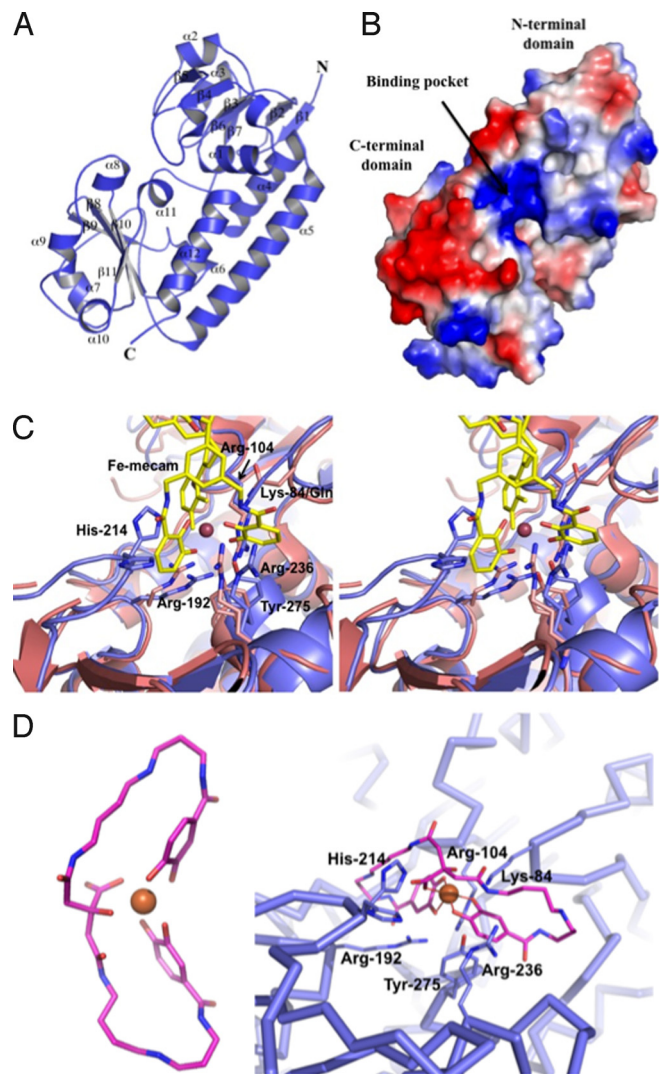


Fig. 4. Structural analysis of YclQ. (A) Ribbon drawing of a YclQ monomer; numbering of secondary structures is shown as α 1–12 and β 1–11. (B) Surface charge potential of YclQ; blue indicates positive and red is for negative. Distinctively, the binding pocket is positively charged to attract $[\text{Fe}(\text{PB})]^{3-}$. (C) Binding site of YclQ shown with the superposed CeuE complexed with $[\text{Fe}(\text{mecam})_2]^{2+}$ in a stereoplot. The conserved residues including Arg and Tyr are shown in stick drawing with gray blue for the YclQ side chains and in magenta for the CeuE side chains; His-214 of YclQ is also shown. (D) (Left) The stick model of FePB (carbon atoms are shown in pink, oxygen atoms in orange, and nitrogen atoms in blue; Fe ion is indicated as an orange ball). (Right) FePB docked into the binding pocket of YclQ shown in an α -carbon tracing. Conserved protein residues potentially interacting with FePB are shown in dark blue sticks with labels. Near the bottom of the pocket, Arg-192 and Arg-104, with minor adjustments, can interact with hydroxyl groups of two 3,4-DHB moieties. Tyr-275 at the bottom of the pocket could stack with one of catechol rings or orient aforementioned Arg residues by contacting with OH. The carboxyl in the citrate moiety may be stabilized by a hydrogen bond with His-214. Lys-84 and Arg-236 are in the neighborhood of spermidine carbonyls to make direct contacts with FePB.

tive wide negatively charged area, perhaps a potential binding site for other proteins involved in iron transport. The two domains are likely to participate in different interactions because in vivo, the N terminus is anchored to the cell membrane via the acetylated C20.

YclQ Binding Pocket Resembles Binding Site of Catecholate Siderophore-Binding PBPs. Among all reported catecholate siderophore-binding PBPs, CeuE is the closest structural homo-

logue of YclQ. The ligand-binding cleft (or pocket) in the YclQ is similar to that of CeuE in size and composition, although CeuE binds 2,3-DHB containing siderophores such as Ent, whereas YclQ binds 3,4-DHB containing PB. To visualize the binding of FePB to YclQ, FePB was energy-minimized and manually modeled into the YclQ structure (Fig. 4D). Overall, FePB is flat with Fe^{3+} lying in plane with the ligand. The splayed orientation of the coordinating oxygens relative to the amide linkage in the 3,4-DHB-binding unit results in a very different 3D complex shape compared with ferric Ent and BB. Furthermore, the mixed citrate/catecholate coordination environment of the iron in FePB is asymmetric (Fig. 4D) in contrast to the tripodal triscatecholate coordination in Ent and BB (34). When the binding pockets of YclQ and CeuE are compared (Fig. 4C), the YclQ conserved residues Arg-104, Arg-192, Arg-236, and Tyr-275 (Fig. S3) assume approximately the same positions as the CeuE conserved residues Arg-118, Arg-205, Arg-249, and Tyr-288, which directly contact ferric mecam (30). In other similar structures, particularly FhuD (1efd) and FeuA (2phz), only Arg-104 and Tyr-275 are well conserved (31, 32). The charge-potential surface drawing of YclQ, with a positively charged pocket to accommodate a negatively charged FePB, is also similar to those of CeuE and FeuA (Fig. 4B). Despite structural similarity and the presence of conserved residues in the YclQ binding site, which should enable hybrid electrostatic/cation- π interactions with the ligands, the spatial arrangement of these residues and the conformation of the pocket are different enough to allow for discrimination between catecholate siderophores with different geometry and atom composition of their metal-binding centers. For example, Lys-121 in CeuE, which interacts with ferric mecam amide oxygen adjacent to catechol ring, corresponds to Glu-107 in YclQ that can potentially make contact with FePB amines. Lys-84 in YclQ (corresponding to Gln-98 in CeuE) is another residue potentially interacting with one of the hydroxyl groups in FePB citrate moiety (Fig. 4D) and possibly conferring ligand specificity. Additionally, the conserved His-214 in the YclQ structure is in two conformations in the right position to interact with FePB by staking or to make a hydrogen bond to the carboxyl group of FePB citrate moiety. The corresponding residue in the CeuE structure is invisible due to disorder in this region of the structure. It is expected that these YclQ residues (Glu-107, Lys-84, and His-214) have roles in specific binding of FePB. These structural differences are likely to be critical for receptor recognition, and the ongoing effort to determine the structures of YclQ complexed with their respective ligands will enable elucidation of these fine differences in ligand specificity.

ESI-MS Elucidates Noncovalent Interactions of YclQ with Siderophores. The formation of noncovalent complexes of the recombinant YclQ with siderophores was monitored by ESI-MS. Following incubation of the YclQ solution in 10 mM ammonium acetate with two equivalents of FePB, the peaks corresponding to the noncovalent YclQ-FePB complex with 1:1 stoichiometry were clearly detectable, in addition to the free protein peaks (Fig. S4A and Table 1). The YclQ complex with the decarboxylated FePB^o was also seen, which confirms that the protein binds both FePB and FePB^o, and the intact citrate backbone is not crucial for receptor recognition (Fig. S4B and Table 1). When the protein was incubated with ferric 3,4-DHB [at a 1:3 ratio of $\text{Fe}:(3,4\text{-DHB})_2$], the complex of $\text{Fe}(3,4\text{-DHB})_2$ with YclQ was observed using LTQ Orbitrap XL (Table 1). A striking observation was made during the ESI-MS analysis of the latter sample using Q-TOF instrument. The mass spectrum showed the presence of the peaks corresponding to the measured mass of 33,519 Da, which suggested that YclQ binds Fe^{3+} , and no protein- $\text{Fe}(3,4\text{-DHB})_2$ complex was detected. Formation of the YclQ-metal complex was confirmed in a sample of YclQ incubated

with Ga^{3+} (3,4-DHB), where peaks corresponding to the YclQ-Ga complex were detected (measured mass of 33,533 Da). The protein was not able to bind metals without the presence of 3,4-DHB, and only the free protein signal was detectable after incubation of YclQ with FeCl_3 . Aromatic amino acids have been shown to form cation- π complexes with alkali and transition metals in the gas phase (35), and we surmise that the Tyr-275 can participate in direct binding of metal in gaseous phase after dissociation of 3,4-DHB from the complex. The possible involvement of Tyr in metal binding would resemble the Fe^{3+} coordination site in iron-binding proteins such as transferrin, lactoferrin, and bacterial periplasmic iron-binding proteins (36). Here the YclQ-Fe complex formation was probably the result of the YclQ-Fe(3,4-DHB)₂ complex dissociation upon transition into gaseous phase. Finally, no YclQ complexes were detected with iron-free PB and 3,4-DHB using ESI-QTOF (Table 1). Because only electrostatic and polar interactions are strengthened in the absence of solvent, this observation indicates that electrostatic forces are involved in the binding of negatively charged ferric PB complexes by YclQ binding-site residues, whereas ionic interactions play a minor role in the binding of apo ligands (37, 38). Additionally, the slightly lower YclQ binding affinity for $[\text{Fe}^{3+}(\text{PB}^{\prime})]^{2-}$ as compared with $[\text{Fe}^{3+}(\text{PB})]^{3-}$ we attribute to the less-negative complex charge rather than the lack of carboxylic group in FePB^{\prime} (Table 1).

Previous Reports on *B. subtilis* YclQ. The receptor YclQ was detected in multiple proteomic studies of *B. subtilis* extracellular proteins from cells grown under various culture and stress conditions, including both iron-poor and iron-rich media, indicating a universal and essential role of this protein in the iron acquisition process (39). Elevated levels of YclQ along with other SBPs were observed in the *B. subtilis fur* mutant (7). YclQ was found not only as a membrane-associated protein but also in the extracellular protein fraction (40). YclQ and other SBPs were found to be released into the medium, which was especially increased in the diacylglycerol transferase mutant, but YclQ was also present at high levels in the wild-type *B. subtilis* 168, due to either membrane leakage or protein shedding by proteolytic shaving (40). This raises the question of whether SBP shedding is not fortuitous, but rather that these proteins participate in scavenging of ferric siderophores in both membrane-tethered and soluble form, similar to the extracellular heme-binding proteins found in other bacteria (41).

Orthologs of YclQ in the *B. cereus* Group. The sequence of the *B. subtilis* SBP YclQ was compared with the ABC-type transporter protein sequences of the *B. cereus* group members, which include PB-producing innocuous and pathogenic strains (15). The BLASTP search showed that the Bcer98_0362 SBP from *B. cereus* subsp. *cytotoxicus* NVH 391–98 shares 59% identity with YclQ, whereas multiple other *B. cereus* and *B. anthracis* strains were found to have SPB proteins that are 25–32% identical to YclQ. Amongst those, the FatB and FpuA proteins from *B. cereus* ATCC 14579 were identified before as PB-binding proteins (20). The FatB ortholog in *B. anthracis* (GBAA5330, 95% identical at the gene level) was the second-most up-regulated gene during germination and early growth stage in host macrophages relative to its *in vitro* growth (42). Because PB is necessary for *B. anthracis* to attain full virulence (16), we expect that the YclQ orthologs in the *B. cereus* group are SBPs of the PB-specific ABC transporters that contribute to virulence of the pathogenic species.

Conclusion

The genus *Bacillus* includes ubiquitous soil and pathogenic species, whose siderophore-mediated iron acquisition systems allow them to thrive in their environments. PB is a siderophore

produced by the members of the *B. cereus* group and has been implicated in the virulence of *B. anthracis*. However, the transport system for this siderophore had not been fully described. The type species *B. subtilis* is among the best understood Gram-positive bacteria, and many aspects of its iron homeostasis are known, including transporters for several xenosiderophores. Identification of YclNOPQ as the PB transporter, and the crystal structure of the YclQ receptor, constitutes a detailed characterization of the PB uptake system in *Bacillus* species. The characterization of the *B. subtilis* PB transporter provides a precedent for better understanding of the virulence-associated PB-mediated iron acquisition systems in pathogenic members of the *B. cereus* group and could be a target in novel antibacterial approaches.

Materials and Methods

Bacterial Strains, Culture Media, and Siderophores. *Bacillus subtilis* 168 (ATCC 6051) was obtained from the American Type Culture Collection. *B. subtilis* disruption mutant strains yclNd (*yclN*::pMUTIN2), yclPd (*yclP*::pMUTIN2), and yclQd (*yclQ*::pMUTIN2) in the strain 168 background were obtained from E. Dervyn (Institut National de la Recherche Agronomique, Paris) (22). Iron-limited medium was prepared as described previously (5). Siderophores were obtained as described previously (20).

Mutant Complementation. The *B. subtilis* yclNd, yclPd, and yclQd mutant strains were complemented with a copy of the corresponding gene under the control of the IPTG-inducible P_{spac} promoter using vector pHCMC05 (Bacillus Genetic Stock Center) (23). The complete *yclQ*, *yclN*, and *yclP* were amplified from *B. subtilis* chromosomal DNA by PCR with primers introducing BamHI and XbaI restriction sites (Table S1). The pHCMC05-*yclN*, pHCMC05-*yclP*, and pHCMC05-*yclQ* constructs were used to transform the corresponding mutant strains of *B. subtilis* yclNd, yclPd, and yclQd using a one-step transformation procedure (43) to obtain the complemented strains yclNd+pHCMC05-*yclN*, yclPd+pHCMC05-*yclP*, and yclQd+pHCMC05-*yclQ*.

⁵⁵Fe-Siderophore Transport Assay. Transport assays in *B. subtilis* 168, yclNd, yclPd, yclQd, and the complemented mutant strains were performed as described previously (5, 20). Data were normalized to 1 mL of bacterial cultures. Detailed protocol is available in *SI Methods*.

Disc Diffusion Assay. These growth assays were performed as described previously with some modifications (44) and are detailed in *SI Methods*.

Cloning, Expression, and Purification of YclQ. The *yclQ* gene lacking the 20-aa N-terminal signal peptide sequence and the subsequent Cys codon predicted for attachment of the diacylglycerol moiety (40) was amplified by PCR from the total DNA of *B. subtilis* 168 using the primers yclQF and yclQR (Table S2) and cloned into a pET101/D-TOPO expression vector introducing a C-terminal His₆-tag (Invitrogen). The TEV protease cleavage site was incorporated into the reverse primer to allow for tag removal using ActEV protease. The cloning and protein expression was performed as described previously, and the YclQ protein was purified using Ni-affinity chromatography (20). Details are available in *SI Methods*.

Fluorescence Spectroscopy. Fluorescence quenching of recombinant YclQ upon binding of siderophores was measured on a Varian Cary Eclipse fluorescence spectrophotometer as described previously (18) and depicted in detail in *SI Methods*. Fluorescence data were analyzed by nonlinear regression analysis of fluorescence response versus ligand concentration using a one-site binding model (24).

Electrospray-Ionization Mass Spectrometry (ESI-MS). The tagless YclQ protein (5 μM) in 10 mM ammonium acetate (pH 6.8) was analyzed using ESI-MS (Q-TOF Premier; Waters) after 2 h incubation with two molar equivalents of ligand solutions. Ferric complexes of ligands (0.1 mM) were prepared *in situ* by combining methanol solution of apo ligands with FeCl_3 or GaCl_3 in 0.1 M HCl in a 1:1 ratio of M:L for PB and 1:3 for 3,4-DHB in 10 mM ammonium acetate (pH 6.8). Additionally, the protein was incubated with two equivalents of FeCl_3 (10 μM). The source parameters were as described previously (20). Additionally, the samples of YclQ incubated with FePB , FePB^{\prime} , and $\text{Fe}(3,4\text{-DHB})$ were analyzed using an LTQ Orbitrap XL (ThermoFisher Scientific) (spray voltage, 2.5 kV; capillary voltage, 30 V; tube lens voltage, 100 V; and capillary temperature, 275 °C).

Cloning, Expression, Purification, and Crystallization of YclQ. To obtain YclQ with a cleavable N-terminal His₆-tag for crystallization trials, the *yclQ* gene lacking the signal peptide sequence was amplified using the primers yclQF-LIC and yclQR-LIC (Table S1) and cloned into pMCSG7 vector as described previously (45). The YclQ proteins from the pET101-*yclQ* and pMCSG7-*yclQ* constructs were expressed in *E. coli* BL21 using selenomethionine (SeMet)-containing enriched M9 medium, and the protein was purified by Ni-affinity chromatography following the protocol described previously (46). The crystallization trials of YclQ were done using a Mosquito robot (TTP Labtech) on sitting drops in 96-well plates (Greiner) at 18 °C (protein concentration of 60 mg/mL). The initial crystals (0.02 × 0.15 × 0.3 mm) of YclQ with the C-terminal His-tag cleaved off appeared after 4 months and diffracted to about 3.0 Å, but twinned. The subsequent streak seeding in similar conditions produced crystals diffracting better than 1.8 Å, which were used for data collection. The details are available in *SI Methods*.

Data Collection, Structure Determination, and Refinement. The single-wavelength anomalous dispersion (SAD) data at the Se peak wavelength 0.9793 Å up to 1.75 Å were collected from a single Se-Met-labeled protein crystal at 100 K on an ADSC Q315 detector at the 19ID beam line of the Structural Biology Center at the Advanced Photon Source, Argonne National Laboratory. All data were processed and scaled with HKL3000 (47) (Table S2).

The structure was determined by SAD phasing using HKL3000 as described previously (48). The initial model was built using the arp/Warp, routine of HKL3000 and Coot, and the subsequent refinement was performed iteratively

by phenix.refine and Coot until it converged to the R factor of 0.158, and the free R of 0.199. The final model with good geometry included residues 14–299 of two chains of YclQ, one phosphate molecule in the PB binding site in one chain, and 509 ordered water molecules. The stereochemistry of the structure was checked with PROCHECK (details in *SI Methods*). Atomic coordinates and experimental structure factors of YclQ have been deposited in the Protein Data Bank (PDB ID code 3GFV).

SI Text. For full experimental details, see *SI Methods*, Figs. S1–S4, and Tables S1 and S2.

ACKNOWLEDGMENTS. We acknowledge helpful discussions on data analysis with Dr. Ulla Andersen and Dr. Petr Kuzmic. Dr. William Eschenfeldt advised on YclQ cloning for crystallization. We thank members of the Structural Biology Center at Argonne National Laboratory for their help with data collection at the 19ID beamline. We acknowledge Dr. Ahmad Gaballa for advice on *B. subtilis* transformation, and thank Drs. Rebecca Abergel and Trisha Hoette for advice and help with manuscript editing. Crude extract of PB was obtained from Prof. B. Rowe Byers (Univ of Mississippi Medical Center, Jackson, MS) and the *B. subtilis* yclNd, yclPd, and yclQd strains were received from Dr. Etienne Dervyn (Institut National de la Recherche Agronomique, Paris). This work was supported by National Institutes of Health Grants AI11744 (to K.N.R.), GM074942 (to A.J.), and 1S10RR022393–01 for the acquisition of the Q-TOF MS, and by the U.S. Department of Energy, Office of Biological and Environmental Research Contract DE-AC02–06CH11357.

- Andrews SC, Robinson AK, Rodriguez-Quinones F (2003) Bacterial iron homeostasis. *FEMS Microbiol Rev* 27:215–237.
- Miethke M, Marahiel MA (2007) Siderophore-based iron acquisition and pathogen control. *Microbiol Mol Biol Rev* 71:413–451.
- Heinrichs DE, Rahn A, Dale SE, Sebulsky MT (2004) Iron transport systems in pathogenic bacteria: *Staphylococcus*, *Streptococcus*, and *Bacillus*. *Iron Transport in Bacteria*, Crosa JH, Mey AR, Payne SM, eds (ASM Press, Washington, DC), pp 387–401.
- Dertz EA, Xu J, Stintzi A, Raymond KN (2005) Bacillibactin-mediated iron transport in *Bacillus subtilis*. *J Am Chem Soc* 128:22–23.
- Dertz EA, Stintzi A, Raymond KN (2006) Siderophore-mediated iron transport in *Bacillus subtilis* and *Corynebacterium glutamicum*. *J Biol Inorg Chem* 11:1087–1097.
- Miethke M, et al. (2006) Ferri-bacillibactin uptake and hydrolysis in *Bacillus subtilis*. *Mol Microbiol* 61:1413–1427.
- Ollinger J, Song K-B, Antelmann H, Hecker M, Helmman JD (2006) Role of the Fur regulon in iron transport in *Bacillus subtilis*. *J Bacteriol* 188:3664–3673.
- Gaballa A, Helmman JD (2007) Substrate induction of siderophore transport in *Bacillus subtilis* mediated by a novel one-component regulator. *Mol Microbiol* 66:164–173.
- May JJ, Wendrich TM, Marahiel MA (2001) The *dhb* operon of *Bacillus subtilis* encodes the biosynthetic template for the catecholic siderophore 2,3-dihydroxybenzoate-glycine-threonine trimeric ester bacillibactin. *J Biol Chem* 276:7209–7217.
- Schneider R, Hantke K (1993) Iron-hydroxamate uptake systems in *Bacillus subtilis*: Identification of a lipoprotein as a part of a binding protein-dependent transport system. *Mol Microbiol* 8:111–121.
- Abergel RJ, Zawadzka AM, Raymond KN (2008) Petrobactin-mediated iron transport in pathogenic bacteria: Coordination chemistry of an unusual 3,4-catecholate/citrate siderophore. *J Am Chem Soc* 130:2124–2125.
- Barbeau K, Zhang G, Live DH, Butler A (2002) Petrobactin, a photoreactive siderophore produced by the oil-degrading marine bacterium *Marinobacter hydrocarbonoclasticus*. *J Am Chem Soc* 124:378–379.
- Koppisch AT, et al. (2005) Petrobactin is a primary siderophore synthesized by *Bacillus anthracis* str. *Sterne* under conditions of iron starvation. *Biomaterials* 18:577–585.
- Wilson MK, Abergel RJ, Raymond KN, Arceneaux JEL, Byers BR (2006) Siderophores of *Bacillus anthracis*, *Bacillus cereus*, and *Bacillus thuringiensis*. *Biochem Biophys Res Commun* 348:320–325.
- Koppisch AT, et al. (2008) Petrobactin is produced by both pathogenic and non-pathogenic isolates of the *Bacillus cereus* group of bacteria. *Biomaterials* 21:581–589.
- Cendrowski S, MacArthur W, Hanna P (2004) *Bacillus anthracis* requires siderophore biosynthesis for growth in macrophages and mouse virulence. *Mol Microbiol* 51:407–417.
- Goetz DH, et al. (2002) The neutrophil lipocalin NGAL is a bacteriostatic agent that interferes with siderophore-mediated iron acquisition. *Mol Cell* 10:1033–1043.
- Abergel RJ, et al. (2006) The anthrax pathogen evades the mammalian immune system through stealth siderophore production. *Proc Natl Acad Sci USA* 103:18499–18503.
- Brown JS, Ogunniyi AD, Woodrow MC, Holden DW, Paton JC (2001) Immunization with components of two iron uptake ABC transporters protect mice against systemic *Streptococcus pneumoniae* infection. *Infect Immun* 69:6702–6706.
- Zawadzka AM, Abergel RJ, Nichiporuk R, Andersen U, Raymond KN (2009) Siderophore-mediated iron acquisition systems in *Bacillus cereus*: Identification of receptors for anthrax virulence-associated petrobactin. *Biochemistry* 48:3645–3657.
- Baichoo N, Wang T, Ye R, Helmman JD (2002) Global analysis of the *Bacillus subtilis* Fur regulon and the iron starvation stimulus. *Mol Microbiol* 45:1613–1629.
- Kobayashi K, et al. (2003) Essential *Bacillus subtilis* genes. *Proc Natl Acad Sci USA* 100:4678–4683.
- Nguyen HD, et al. (2005) Construction of plasmid-based expression vectors for *Bacillus subtilis* exhibiting full structural stability. *Plasmid* 54:241–248.
- Kuzmic P (1996) Program DYNAFIT for the analysis of enzyme kinetic data: Application to HIV proteinase. *Anal Biochem* 237:260–273.
- Sebulsky MT, Shilton BH, Speziali CD, Heinrichs DE (2003) The role of *fluD2* in iron(III)-hydroxamate transport in *Staphylococcus aureus*. Demonstration that FluD2 binds iron(III)-hydroxamates but with minimal conformational change and implication of mutations on transport. *J Biol Chem* 278:49890–49900.
- Stintzi A, Barnes C, Xu J, Raymond KN (2000) Microbial iron transport via a siderophore shuttle: A membrane ion transport paradigm. *Proc Natl Acad Sci USA* 97:10691–10696.
- Garner BL, Arceneaux JEL, Byers BR (2004) Temperature control of a 3,4-dihydroxybenzoate (protocatechuate)-based siderophore in *Bacillus anthracis*. *Curr Microbiol* 49:89–94.
- Calugay RJ, et al. (2006) Catechol siderophore excretion by magnetotactic bacterium *Magnetospirillum magneticum* AMB-1. *J Biosci Bioeng* 101:445–447.
- Ho WW, et al. (2007) Holo- and Apo-bound structures of bacterial periplasmic heme-binding proteins. *J Biol Chem* 282:35796–35802.
- Müller A, Wilkinson AJ, Wilson KS, Duhme-Klair AK (2006) An $[(\text{Fe}(\text{mecam}))_2]^{6-}$ bridge in the crystal structure of a ferric enterobactin binding protein. *Angew Chem Int* 45:5132–5136.
- Clarke TE, Ku S-Y, Dougan DR, Vogel HJ, Tari LW (2000) The structure of the ferric siderophore binding protein FluD complexed with gallichrome. *Nat Struct Biol* 7:287–291.
- Clarke TE, Braun V, Winkelmann G, Tari LW, Vogel HJ (2002) X-ray crystallographic structures of the *Escherichia coli* periplasmic protein FluD bound to hydroxamate-type siderophores and the antibiotic albomycin. *J Biol Chem* 277:13966–13972.
- Evdokimov AG, Anderson DF, Routhahn KM, Waugh DS (2001) Structural basis for oligosaccharide recognition by *Pyrococcus furiosus* maltodextrin-binding protein. *J Mol Biol* 305:891–904.
- Dertz EA, Raymond KN (2004) Biochemical and physical properties of siderophores. *Iron Transport in Bacteria*, eds Crosa JH, Mey AR, Payne SM (ASM Press, Washington, DC), pp 5–17.
- Rezabal E, Marino T, Mercero JM, Russo N, Ugalde JM (2007) Complexation of Al^{III} by aromatic amino acids in the gas phase. *Inorg Chem* 46:6413–6419.
- Baker HM, Anderson BF, Baker EN (2003) Dealing with iron: Common structural principles in protein that transport iron and heme. *Proc Natl Acad Sci USA* 100:3579–3583.
- Loo JA (2000) Electrospray ionization mass spectrometry: A technology for studying noncovalent macromolecular complexes. *Int J Mass Spectrom* 200:175–186.
- Rockwood AL, Busman M, Smith RD (1991) Coulombic effects in the dissociation of large highly charged ions. *Int J Mass Spectrom Ion Process* 111:103–129.
- Bunai K, et al. (2004) Profiling and comprehensive expression analysis of ABC transporter solute-binding proteins of *Bacillus subtilis* membrane based on a proteomic approach. *Electrophoresis* 25:141–155.
- Antelmann H, et al. (2001) A proteomic view on genome-based signal peptide predictions. *Genome Res* 11:1484–1502.
- Maresso AW, Garufi G, Schneewind O (2008) *Bacillus anthracis* secretes proteins that mediate heme acquisition from hemoglobin. *PLoS Pathog* 4:e1000132.
- Bergman NH, et al. (2007) Transcriptional profiling of *Bacillus anthracis* during infection of host macrophages. *Infect Immun* 75:3434–3444.
- Jarmer H, Berka R, Knudsen S, Saxild HH (2002) Transcriptome analysis documents induced competence of *Bacillus subtilis* during nitrogen limiting conditions. *FEMS Microbiol Lett* 206:197–200.
- Lee JY, et al. (2007) Biosynthetic analysis of the petrobactin siderophore pathway from *Bacillus anthracis*. *J Bacteriol* 189:1698–1710.
- Stols L, et al. (2002) A new vector for high-throughput, ligation-independent cloning encoding a tobacco etch virus protease cleavage site. *Protein Express Purific* 25:8–15.
- Kim Y, et al. (2004) Automation of protein purification for structural genomics. *J Struct Funct Genomics* 5:111–118.
- Minor W, Cymborowski M, Otwinowski Z, Chruszcz M (2006) HKL-3000: The integration of data reduction and structure solution—From diffraction images to an initial model in minutes. *Acta Crystallogr D Biol Crystallogr* 62:859–866.
- Pfleger BF, et al. (2008) Structural and functional analysis of AsbF: Origin of the stealth 3,4-dihydroxybenzoate subunit for petrobactin biosynthesis. *Proc Natl Acad Sci USA* 105:17133–17138.